Journal of Biomedical Optics 9(4), 691–699 (July/August 2004)

Applications of digital image correlation to biological tissues

Dongsheng Zhang*
Shanghai University
Department of Mechanics
99 Shangda Road
Shanghai, 200436 China

Dwayne D. Arola
University of Maryland Baltimore County
Department of Mechanical Engineering
1000 Hilltop Circle
Baltimore, Maryland 21250

Abstract. Optical methods are becoming commonplace in investigations of the physical and mechanical behavior of biological tissues. Digital image correlation (DIC) is a versatile optical method that shows tremendous promise for applications involving biological tissues and biomaterials. We present the fundamentals of DIC with an emphasis on the application to biological materials. An approach for surface preparation is described that facilitates its application to hydrated substrates. Three examples are presented that highlight the use of DIC for biomedical research. The first example describes the use of DIC to study the mechanical behavior of arterial tissues up to 40% elongation. The second example describes an evaluation of the mechanical properties of bovine hoof horn in the dehydrated and fully hydrated states. Uniaxial tension experiments are performed to determine the elastic modulus (E) and Poisson's ratio (ν) of both the arterial and dermal tissues. Spatial variations in the mechanical properties are evident from the full-field characterization of both tissues. Finally, an application of DIC to study the evolution of loosening in cemented total hip replacements is described. The noncontact analysis enables measurement of the relative displacement between the bone/bone cement and bone cement/prosthesis interfaces. Based on the elementary optical arrangement, the simple surface preparation, and the ability to acquire displacement/strain measurements over a large range of deformation, DIC should serve as a valuable tool for biomedical research. Further developments will enable the use of DIC for *in vivo* applications.
[DOI: 10.1117/1.1753270]

Keywords: digital image correlation; biological tissue; interferometry.

Paper 03007 received Jan. 22, 2003; revised manuscript received Jun. 9, 2003, and Dec. 2, 2003; accepted for publication Dec. 5, 2003.

1 Introduction

An understanding of the mechanical behavior of soft and hard tissues is often valuable in the diagnosis of disease and in the design of new biomaterials that are developed to maintain lifelong health. The mechanical behavior of engineering materials can be evaluated using a number of methods that are based on either contact or noncontact schemes for displacement measurement. Optical techniques have proven valuable in characterizing the properties of advanced materials, especially those systems exhibiting anisotropy or inhomogeneity. But the physical and mechanical properties of tissues are generally more difficult to evaluate than those of conventional or even advanced engineering materials. The necessity of maintaining hydration, the size or geometric limitations of available tissue samples, and difficulties encountered in the fabrication of specimens pose serious challenges. Consequently, there has been considerable interest in using optical methods to characterize the mechanical behavior of biological tissues.

Optical techniques based on laser illumination and interferometry have been adopted for biomechanics research in medicine and dentistry. Some noteworthy examples include the use of holographic interferometry to identify soft tissue abnormalities,[1] to evaluate structural changes posed by the placement of orthopedic devices,[2,3] and to enhance the efficacy of medical and dental practices.[4–6] Geometric Moiré, Moiré interferometry, and electronic speckle pattern interferometry (ESPI) have also been used to study the properties of hard tissues such as bone[7,8] and the dentin and enamel of teeth.[9–11] Laser-based optical methods for displacement measurement are very precise and typically capable of resolving submicrometer displacements. However, the measurement range is often small ($\leqslant 100\ \mu$m), which has limited their application to the study of hard tissues or the evaluation of soft tissues over a limited range of deformation.

Many soft tissues undergo moderate deformation *in vivo*, which exceeds the range of measurement available from interferometric techniques. An additional concern in application of interferometric or laser-based techniques is the complex surface preparation required to achieve reflection and interference on hydrated samples.[12] Natural hydration of most tissues requires that both the surface preparation and evaluation are conducted without dehydration.

*Author to whom all correspondence should be addressed. Currently a Senior Research Scientist in the Department of Mechanical Engineering at the University of Maryland Baltimore County.

1083-3668/2004/$15.00 © 2004 SPIE

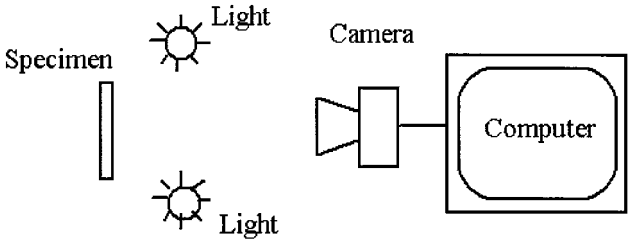

Fig. 1 Schematic diagram of equipment for DIC.

A complete review of optical techniques and their applications in medicine and dentistry is beyond the scope of this paper. Recently, a new optical method has been established that overcomes many of the aforementioned limitations of laser-based and interferometric techniques in application to tissues. Digital image correlation (DIC) is a noncontacting, flexible optical method for displacement and strain measurement that has been widely applied in engineering and scientific research.[13] It has been adopted to measure the displacement/strain distribution in engineering structures[14–16] and in determinations of the mechanical properties of engineering materials.[17–20] With appropriate image processing, DIC is capable of quantifying large strains ($\geqslant 50\%$) and, therefore, has been used to document plastic deformation of materials.[21,22] Yet, surprisingly, reported applications of DIC in the evaluation of biological materials are rather limited.

In this paper, the fundamentals of DIC are introduced, including method of surface preparation, data acquisition, and data reduction. Where appropriate, special emphasis is placed on applications to biological tissues. Examples are then presented illustrating three different applications of DIC in evaluating the mechanical behavior of biological materials and biomaterials. The advantages of DIC over other techniques in applications to biological materials are then summarized.

2 DIC

DIC is a unique optical technique that uses image recognition to analyze and compare digital images acquired from the surface of a substrate. A typical experimental arrangement for DIC is shown in Fig. 1. An incoherent light source is used to illuminate the object's surface uniformly and a CCD camera or a digital camera is placed normal to the illuminated surface. Two images are acquired, one taken ''before'' and one ''after'' the deformation that results from mechanical and/or thermal loads. The two images are digitized and stored on a computer for further processing.

With proper surface preparation, the interaction between the incident light and the object surface results in an image with random, high-contrast, and high-frequency variations in light intensity; the surface appears ''speckled.'' Digital images acquired before and after deformation document the ''speckle'' distribution and can be represented by the gray-scale intensity distribution. The light intensity distribution at each point on the surface is unique and the distribution in light intensity about a particular point (x,y) can be described by the grayscale matrix $F(x,y)$ over a selected subset of the digital image. With deformation of the object each position of the surface (x,y) is assumed to exist at a new location (x^*,y^*). The in-plane surface displacement can be determined by finding the position of the light intensity distribution $F^*(x^*,y^*)$ that most closely resembles the original distribution $F(x,y)$. A search is performed to find the location on the ''deformed'' image (after deformation) with the gray-scale distribution that is most consistent with that on the original ''undeformed'' image. The location of $F^*(x^*,y^*)$ can be obtained by finding the position with maximum correlation coefficient (C) according to

$$C=\frac{\langle \mathbf{F}\mathbf{F}^*\rangle-\langle \mathbf{F}\rangle\langle \mathbf{F}^*\rangle}{[\langle(\mathbf{F}-\langle \mathbf{F}\rangle)^2\rangle\langle(\mathbf{F}^*-\langle \mathbf{F}^*\rangle)^2\rangle]^{1/2}}, \tag{1}$$

where $\mathbf{F}$ and $\mathbf{F}^*$ are the gray-scale matrices of the subset at position (x,y) in the undeformed image and (x^*,y^*) in the deformed image, respectively. The symbol $\langle\,\rangle$ in Eq. (1) implies the mean value of the elements in the matrix. The search for the point with maximum correlation coefficient $(C_{\max})$ on the deforemed image is initially implemented at integer pixel locations until the location with the maximum correlation coefficient is found. The classic cross-correlation method has proven to be efficient and robust in conducting a correlation search.[14,15] For an increase in precision, the search can be continued in the subpixel domain about that integer pixel with maximum correlation coefficient. To increase precision the search for location with maximum correlation can be continued from the integer pixel in successive search steps from 0.1 pixels to 0.01 pixels to a final step of 0.001 pixels. Thus, a precision of 0.001 pixels can be achieved. There are different search strategies available, the most common of which is the Newton-Raphson method.[23] In all examples presented in this paper, the fast-search strategy was employed.[24]

The surface displacements are determined from the positions of the gray-scale distribution of the deformed image with respect to that of the original image. If the out-of-plane displacement is small and can be neglected, the location in the deformed image (x^*,y^*) is described by

$$x^*=x+u+\frac{\partial u}{\partial x}\Delta x+\frac{\partial u}{\partial y}\Delta y,$$

$$y^*=y+v+\frac{\partial v}{\partial x}\Delta x+\frac{\partial v}{\partial y}\Delta y, \tag{2}$$

where u and v are the displacements of the subset center in the x and y directions, respectively. In traditional DIC the quantities $u,v,\partial u/\partial x,\partial v/\partial y,\partial u/\partial y$, and $\partial v/\partial x$ are evaluated iteratively and determined from the position with maximum correlation coefficient [Eq. (1)]. However, since the displacements are much greater than the corresponding partial derivatives, the process can be simplified if only the displacements are obtained from correlation and the strain is determined from the first derivatives according to

$$\varepsilon_x=\frac{\mathrm{d}u}{\mathrm{d}x},$$

$$\varepsilon_y=\frac{\mathrm{d}v}{\mathrm{d}y}. \tag{3}$$

Note from the terms $\mathrm{d}u$ and $\mathrm{d}v$ in Eq. (3) that the contribution of rigid body motion in the x and y directions will be auto-

matically eliminated. The cross-correlation function is sensitive in detecting in-plane rotation that is[18] less than 10 deg. If the in-plane rotation is more appreciable, there are other correlation schemes that can be employed to detect the contribution of the rotation. The out-of-plane displacement should be limited to the deformation resulting from Poisson effects. To minimize the effects of out-of-plane displacement the distance between the camera lens and substrate should be maximized. Yet, care must be taken to avoid sacrificing measurement resolution due to the corresponding reduction in image magnification.

Two primary features of the speckle field influence the robustness and precision of deformation measurements; namely, the gray-scale variation and the speckle size. The gray-scale range between speckles and background should enable the digitized gray-scale distribution of a subset to have its own unique distribution that can be recognized by the cross-correlation equation after deformation. Thus, it is advantageous to increase the contrast of the speckle field or the gray-scale difference between speckles and background. A substrate with inadequate contrast will raise the potential for ''false'' correlation [i.e., the correlation coefficient is close to 1.0 according to Eq. (1), but the images before and after deformation do not correspond to the same locations on the substrate]. Unless the substrate exhibits a surface with natural speckles and high contrast, a surface treatment is mandatory and will depend on the tissue, level of hydration, and desired precision.

The spray method is an effective and relatively quick surface preparation for hydrated tissues that are light in color. The process consists of depositing a fine mist of black enamel paint, which results in a random pattern of black dots. A fast-drying paint is desired to minimize the potential for chemical contamination of the tissue. For tissues that are either semi-transparent or dark, a matte white background should be prepared prior to depositing the final coating of black dots. A thin uniform coat of white enamel paint can be used for the background. For most hard tissue samples, a thin coat of liquid paper is also suitable for the background. In general, the size of the sprayed dots can limit the precision of the displacement measurement; the dot size must be smaller than the subset size that is chosen for image correlation. Adjusting the distance between the specimen's surface and spray nozzle (of the aerosol can) can be used to regulate the deposited speckle size; generally the speckle size decreases with an increase in distance to the target. Spraying peripherally, rather than directly at the target, can be used to reduce the speckle size even further. A typical speckle pattern resulting from preparation of an arterial wall using the spray method is shown in Fig. 2. Note that the speckle size must be occupy an area smaller than the correlation window. If a correlation window of 21 $\times$21 pixels is used, a suitable speckle must have an effective diameter of $\leqslant$20 pixels. The perceived speckle size in the image is inversely proportional to the field of view of the camera (i.e., a larger field of view results in a smaller apparent speckle size). The speckle size does not have a direct relationship with the spatial resolution of the image system, but decorrelation may occur if the speckle size is larger than the subset window. Therefore, the speckle size deposited by the spray technique must be less than the size of the subset chosen for the correlation windows. For instance, in a field of view of 25.4$\times$20 mm documented with spatial resolution of 640 $\times$480 pixels, the sprayed speckle size should be less than 0.8 mm (for a correlation window of 21$\times$21 pixels). Larger speckle sizes may make it necessary to use a larger subset size to maintain correlation. As a consequence, the correlation process requires a greater computational time. Assuming that the search for position with maximum correlation is continued from the pixel to the subpixel domain, DIC can provide displacement measurement with precision up to $\pm$0.01 pixels.

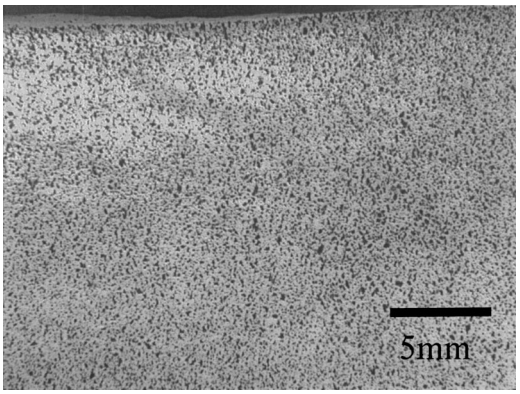

Fig. 2 Typical speckle image prepared for DIC.

3 Calibration

In evaluating the constitutive behavior of biological materials there are often limited reliable sources available for verification of results. Consequently, it is valuable to perform a series of benchmark experiments that serve as a means of calibration. An exercise of this type is especially important in adopting the use of new measurement techniques. In this regard, we performed experiments using silicon rubber (40 Durometer) as a model material and compared the mechanical behavior estimated using DIC with that obtained using conventional techniques for measurement of elongation. Rectangular sections were obtained from a silicon rubber sheet with dimensions of 25.4$\times$85 mm and 1.6 mm thickness. A speckle pattern was generated on the surface of the rubber specimens using the spray technique. The mechanical behavior was evaluated under uniaxial tension using a universal testing system (Instron Dynamite Universal Testing System, Model 8841, Canton, Massachusetts) with full-scale range of 1000 N. Uniaxial loads were applied under displacement control actuation to a maximum of 50% elongation at strain rate 5 $\times 10^{-4}$ s^{-1}. An image size of 25$\times$18 mm was acquired centrally with regards to the clamped edges using a digital camera with resolution of 1280$\times$960 pixels with 256 gray levels. The effective gage length for the axial strain measurements using DIC was 25 mm. The axial strain was also monitored using a miniature extensometer (Epsilon miniature extensometer, Model 3442, Jackson, Wyoming) with a 6-mm gage length and a maximum elongation of 25%. The axial response was quantified in terms of the true stress and Lagrangian strain, which is defined according to

$$\varepsilon_x = u_x + \frac{u_x^2 + v_x^2}{2},$$

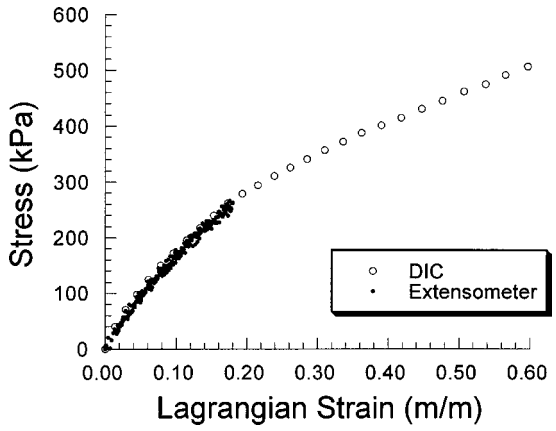

Fig. 3 Axial response of the rubber evaluated using displacement measurements from DIC and the extensometer.

$$\varepsilon_y = v_y + \frac{u_y^2 + v_y^2}{2},$$

$$\gamma_{xy} = \frac{u_y + v_x}{2} + \frac{u_x u_y + v_x v_y}{2}. \quad (4)$$

The strains were estimated using both methods of displacement measurement (i.e., DIC and extensometer). In reporting the axial and transverse strains using DIC, the axial and transverse strains were estimated from the average of the respective components over the entire image area (18×25 mm).

A comparison of the uniaxial behavior for the silicon rubber determined using both methods of measurement is shown in Fig. 3. As is evident from the stress-strain response, the extensometer was limited to 25% elongation, whereas the axial strain deduced using DIC was documented to over 50% elongation. The stress-strain response estimated from DIC agrees well with that from the electromechanical extensometer.[25] The largest error ($\sim 2\%$) occurred at small strains ($\varepsilon \leqslant 5\%$) and was evident from a comparison of the Poisson ratio for the silicon rubber with that dictated by conservation of volume ($v = 0.5$). Out-of-plane displacement of the specimen at the onset of loading was primary responsible for the error. Out-of-plane displacement causes defocusing and decorrelation of the speckles due to the perceived changes in speckle shape[14] and can be especially troublesome in the evaluation of compliant materials.

Results from the cursory experiments indicate that errors in displacement measurement (and corresponding mechanical behavior) determined using DIC are the largest at small strain; that is, a recognized limitation of DIC with respect to the precision offered by other optical techniques. Based on a comparison of the correlation coefficients resulting from the analysis of silicon rubber with that resulting from a similar analysis of hydrated tissue[25] it was found that the image correlation process was not influenced by the difference in surface hydration. The correlation coefficients for the rubber and tissue were found to be nearly identical at the same quantity of relative axial strain.[25] Therefore, the simple method of surface preparation used is an effective way to generate speckle patterns that support use of DIC. It is also relatively insensitive to whether the surface is wet or dry. Thus, there is clearly an advantage of using DIC based on the increased range of deformation documented, the opportunity to quantify the axial and transverse strains simultaneously, and the ability to conduct a full-field evaluation.

4 Applications

The fundamentals of DIC were presented including a description of surface preparations that are appropriate for use on biological tissues. An approach for benchmarking was then introduced that utilizes a model material. In this section, three examples are presented that illustrate application of DIC to biological tissues and biomaterials.

The applications described in this manuscript utilized two different optical systems. An Olympus C 3000Z digital camera and a Panosonic WV-BP550 black and white video camera combined with a Computar 10× zoom lens were used for specific applications. The Olympus digital camera has a built-in 3× optical and 2.5× digital magnification. To obtain higher magnification a set of PROMASTER close-up lenses was attached in front of the built-in lens. Use of the close-up lens can effectively avoid image aberration in close-range image acquisition. The spatial resolution of the Olympus can be adjusted from 1280×960 to 2048×1536 pixels, whereas the spatial resolution for the video camera is fixed at 640×480 pixels. In all applications where image resolution was a primary concern or large gradients in the displacement and corresponding strain distribution were expected, the digital camera was chosen to acquire images.

4.1 *Mechanical Properties of the Bovine Artery*

Stroke ranks as the third leading cause of death and the leading cause of long-term disability. The prevalent cause for stroke is the rupture of unstable atherosclerotic plaque within the sinus of the carotid artery that provides blood to the brain. To reduce the risk of stroke, it is essential to understand the mechanical conditions and consequent stress distribution in arterial walls that facilitate plaque rupture. As a first step, we adopted the use of DIC to determine the mechanical properties of the arterial wall.[25–28] Previous studies on arterial tissues have used the ''marker method,'' which utilizes the change in location of three or four discrete marker points to extract the in-plane strain.[29–30] One outstanding drawback is that the mechanical response of the tissue becomes homogenized over the marker grid. Arterial tissue is composed of layers of elastin and collagen and there is a high degree of nonlinearity in response to large strain.[31] Local variations in the anisotropy and inhomogeniety of arterial tissues have not been examined in detail, partly due to the limitations of traditional experimental approaches.

In this preliminary study, bovine aorta and descending artery (total length from aortic arch of approx. 20 cm) were obtained within 1/2 h post mortem and maintained in saline solution. The arteries were maintained in an ethylene glycol tetra-acetic acid (EGTA) enhanced passive physiologic solution except during transport, dissection and testing. Each artery was cut axially between the thoracic ostia and laid flat, intimal side up. Rectangular specimens were excised, oriented axially, measuring approximately 25×100 mm. Specimens with a uniform thickness of approximately 2.0 mm were removed using a microtome blade, yielding arterial sections

comprised of the intima and medial layers. The methodology used for specimen preparation is consistent with that used by previous investigators.[31] Sectioning of the arterial samples using the microtome may have influenced the structural behavior of the tissue; damage to the tissue may have resulted from the sectioning process but was ignored. Prior to loading, each specimen was taken out of the EGTA solution and excess moisture on the intimal surface was wiped gently with a paper tissue. As the intimal surface is matte white, a peripheral coat of black enamel paint (Rustoleum) was sprayed directly on the surface to generate a high-contrast speckle pattern. The enamel paint contains solvents that may affect the properties of the tissue, but due to the small coating thickness and short period of testing time ($t \leqslant 30$ min), the potential influence was ignored. In addition, the speckles were nearly dry on contact with the tissue, which further limited potential effects from the solvent. After deposition, there was minimal evidence of running or diffusion of the paint.

The specimens were placed within a dedicated load frame and subjected to uniaxial monotonic tensile loads under displacement control actuation. Compression grips were used to clamp both ends of the specimens and the average gage length between grips was 75 mm. Displacement increments of 1.27 mm (0.05 in.) were applied to the aorta sections until reaching a maximum axial deformation of 25 mm. The reaction load resulting from elongation was determined using a precision load cell with full-scale range of 22.5 N. An image of the specimen's surface was recorded prior to loading and at each step of axial displacement. The tension experiments for the arterial specimens were comprised of loading the specimen to 25% nominal elongation and unloading 12 times consecutively. The 13th and 14th cycles consisted of loading to 30 and to 40% elongation and unloading, respectively. The first 12 cycles were conducted to condition the samples and achieve a steady state mechanical response. Speckle images were documented during the 1st, 4th, 8th, 12th, 13th, and 14th cycles at every 2% elongation along with the corresponding axial load. A typical experiment comprised of the 14 load-unload cycles with one specimen required about 30 min.

An image size of 25×18 mm was utilized and digitized into a sample of 1280×960 pixels with 256 gray levels. A comparison of the digitized speckle distributions captured at each load step was conducted to determine the full-field displacement by means of DIC. The strain distribution was then calculated from the displacement distribution according to Eq. (4). A typical stress/strain response for an arterial section at the 14th cycle is shown in Fig. 4(a). The elastic moduli for the axial sections of arterial wall were determined using the tangent method from the stress and strain relations in each cycle and using the average strain over the entire window of evaluation. The average primary (E_1) and secondary (E_2) elastic moduli for the arterial specimens was 192 and 912 kPa, respectively. An example of the axial strain distribution over the surface of the tissue at 40% elongation is shown in Fig. 4(b). Note the distinct patterns in strain distribution, as evident from the gray-scale variation. The coefficient of variation in displacement and corresponding strain was approximately 0.16 regardless of the degree of elongation. The elastic modulus reported for specimens comprised of intimal and medial layers of the descending aorta is[32] 248 kPa. Mechanical properties of arteries are dominated by the medial layer as it is

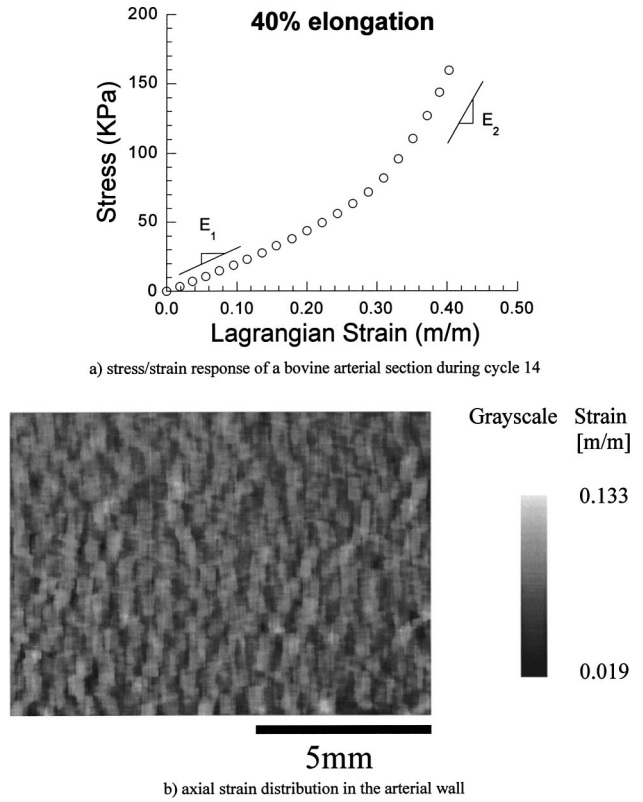

Fig. 4 Typical response of a bovine artery subjected to uniaxial tension: (a) stress/strain response of a bovine arterial section during cycle 14 and (b) axial strain distribution in the arterial wall.

comprised of the highest percentage of collagen fibers. The specimens examined in this study were comprised of the intima and a portion of the media; the average elastic modulus after conditioning was 192 kPa. Based on the difference in ratio of intimal to medial components, it is reasonable that the elastic modulus was less than that reported in the literature. Note, however, that the axial stress was calculated using actual cross-sectional area, based on the assumption that volume is preserved.

With proper surface preparation of the substrate, DIC provides a useful method for evaluating the constitutive behavior of soft tissues over a large range in strain. Based on results from the analysis of bovine aorta, DIC can be used to examine the constitutive behavior of soft tissues and the variability that may result from structural variations or pathogenesis. It was also found that DIC is relatively insensitive to whether the surface is wet or dry.[25] The full-field characterization enabled by DIC may provide new knowledge regarding the structure/property relationship for arterial tissues.

4.2 *Mechanical Behavior of Bovine Hoof Horn*

Lameness of dairy cows resulting from hoof and leg ailments is a major problem in the dairy industry. A preliminary study of the effects of moisture on the elastic properties of bovine hoof horn was recently conducted to evaluate the potential effects of evolving dairy conditions on hoof injuries.[33,34] Hooves were obtained from mature Holstein and Black Angus cows within 12 h of sacrifice. Thin uniform slices of approximately 0.5 mm were excised incrementally from the sole to-

(a) excising thin sections from hoof claw

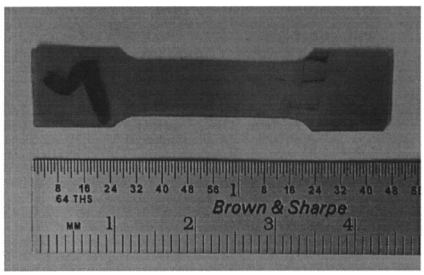

(b) geometry of typical tension specimens stamped from the serial sections

Fig. 5 Preparing tensile specimens from the sole of cow hooves: (a) excising thin sections from hoof claw and (b) geometry of typical tension specimens stamped from the serial sections.

ward the dermal-epidermal junction of both the lateral and medial claws of the front and rear hooves. Conventional dog-bone tensile specimens were then stamped from the individual slices, as shown in Fig. 5(a). In this preliminary study, the elastic properties were evaluated according to two levels of hydration, which were achieved according to specific storage conditions. All specimens were stored dry at 4 °C for a period no less than 1 week; the ''dry'' samples were stored in air while the ''wet'' samples were maintained in a bath of deionized water. Although the moisture content was not quantified, the specimens were considered dehydrated and fully saturated (100% relative humidity). According to the natural pigmentation of hoof horn, the raw specimens were dark gray or black. After removing the specimens from storage, a thin uniform coat of matte white enamel paint was sprayed over the gauge section and was followed by a peripheral coating of black enamel paint. The combination resulted in a high-contrast speckle distribution suitable for DIC. All samples were tested immediately after removal from storage.

The hoof horn specimens were subjected to uniaxial tension under displacement control using a universal testing machine (Instron Dynamite Universal Testing System, Model 8841, Canton, Massachusetts). Displacement increments of 1.27 mm (0.05 in.)/min were applied to the specimens until reaching a maximum axial load of 20 N or failure of the specimen. The reaction load resulting from elongation was determined using a precision load cell with full-scale range of 22.5 N. The image capturing system was initialized by a trigger signal originating from the universal test machine at the onset of loading. Sequential images with spatial resolution of 640×480 pixels and 256 gray scales were captured from an evaluation window of 8.5×6.4 mm every 2 s until reaching an axial load of 20 N or failure of the specimen. The displacement/strain distribution can be deduced using DIC in one of two ways. One is to analyze each image in real time while the images are being documented. In this manner, the amount of pixels being analyzed is limited by the computer's processing speed and the time interval between sequential images. The other approach is to store the sequential images onto the hard drive while performing the tension experiments and then to process them consecutively after the experiment. The second approach was adopted as the strain can be deduced with increased precision using a larger subset area for establishing correlation.

A typical stress/strain response for wet and dry specimens is shown in Fig. 6(a). The elastic moduli for the specimens in both dry and wet conditions was determined from the elastic response for strains less than 0.1% using the tangent method. The average elastic modulus of the ''dry'' hoof horn was 2870 ± 460 MPa, which is significantly larger than that of the ''wet'' horn ($E=102\pm34$ MPa). Results from this preliminary study indicate that environmental conditions at the dairy farm may be important to the stiffness of cow hoof horn and reductions in stiffness with increasing moisture may raise the potential for hoof injuries. Poisson's ratios for the hoof horn specimens in the two conditions (wet and dry) are shown in Fig. 6(b). Note that the largest variation in Poisson's ratio occurs at the onset of axial loading and is attributed to the small transverse component of displacement. Similar to the stiffness, Poisson's ratio for the hoof horn is a function of the moisture content and the implications of this change on hoof health remain to be addressed. A typical full-field description of the axial strain distribution over the entire window of evaluation (8.5×6.4 mm) for a tensile specimen is shown in Fig. 6(c). Similar to the strain distribution for the bovine artery, there are distinct variations in the axial strain indicating an inhomogeneous distribution in the mechanical properties. The variation in strain is evident from the gray-scale map and suggests that there are abnormalities of the tissue. The average coefficient of variation in the axial strain distribution for all specimens was 0.18. Using the full-field characterization available from DIC it is possible to establish stochastic descriptions for the elastic properties of cow hoof horn and to define the mechanical behavior as a function of the hoof anatomy. These valuable details will be examined in future studies.

4.3 *Loosening in Cemented Total Hip Replacements*

Loosening of the femoral component in total hip replacements (THR) is one of the most common sources of hip replacement failure. The influence of bone surface preparation on the mechanics of loosening in cemented joint replacements was studied. The investigation relies on the use of DIC to identify changes in relative displacement between the bone, cement, and prosthesis of model THR systems.[35,36]

All experiments were conducted with fresh bovine femurs obtained within 12 h of sacrifice. The middiaphyseal portion of the femur was sectioned to obtain a specimen 66 to 76 mm in length. Sections with relatively uniform canal diameter ($d<30$ mm) and a thick wall ($t>7$ mm) were then selected for further preparation and evaluation. The sectioned bone was milled to 63.5 mm long, and the canal diameter was increased

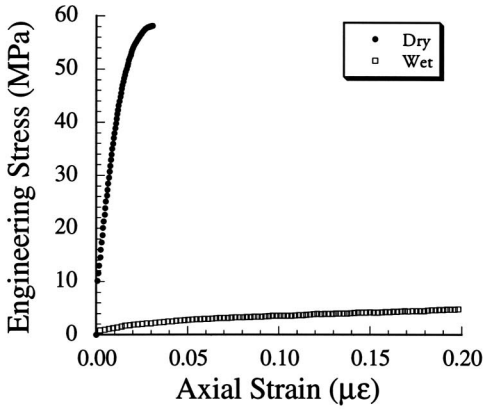

a) typical stress/strain response for wet and dry hoof horn.

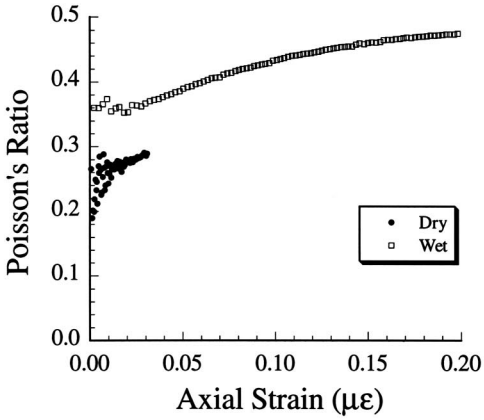

b) Poisson's ratio for the wet and dry specimens from 6(a)

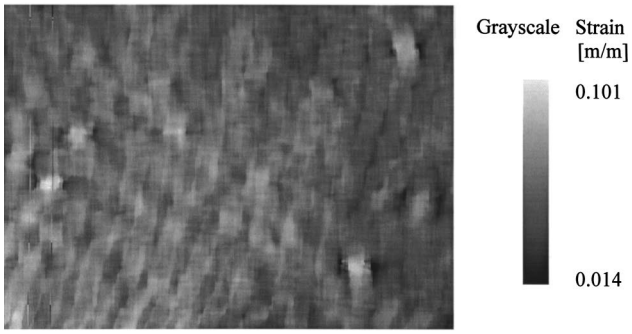

c) strain distribution of wet cow hoof horn under uniaxial tension

Fig. 6 Mechanical behavior of the hoof horn established using DIC: (a) typical stress/strain response for wet and dry hoof horn, (b) Poisson's ratio for the wet and dry specimens form (a), and (c) strain distribution of wet cow hoof horn under uniaxial tension

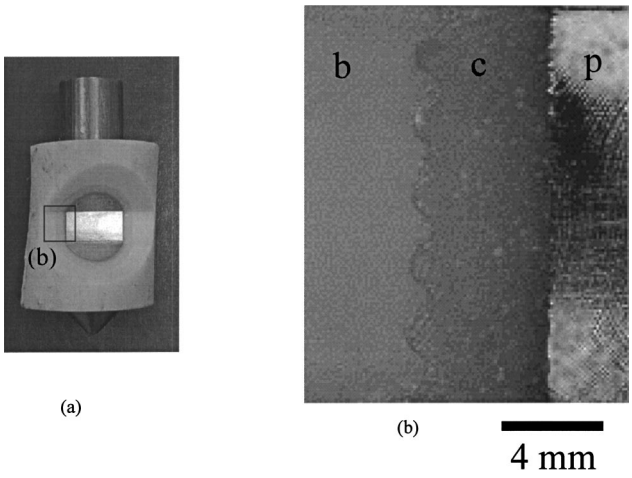

(a) (b)

Fig. 7 Model femoral hip replacement with titanium prosthesis (*b* = bone, *c* = cement, *p* = titanium prosthesis): (a) model implant with evaluation window revealing the prosthesis/cement and cement bone interfaces and (b) the interfaces of the specimen in (a) with specific bone surface preparation.

to 31.8 mm, using a specific tool chosen to impart a desired surface profile and corresponding roughness. A model commercially pure titanium (CPTi) prosthesis is then inserted within the prepared femoral section and cemented in place using polymethylmethacrylate (PMMA) bone cement (DePuy Endurance® PMMA bone cement, Warsaw, Indiana) and advanced cementing techniques (water lavage and cement pressurization). The CPTI prosthesis has a 25.4-mm diameter and knurled surface to simulate the rough texture of a real prosthesis. Dimensions of the femoral canal and prosthesis result in a cement mantle thickness of approximately 3.2 mm. Although the prosthesis morphology is slightly different than that of commercial devices, it provides an adequate model with which to reconstruct the cemented total hip replacement.

The cemented joints were further modified to enable an examination of the interface displacement. An evaluation window was milled in two opposing sides of the specimen [Fig. 7(a)] to reveal the cement/bone and cement/prosthesis interfaces [Fig. 7(b)]. Flaws may be introduced within the cement during machining of the evaluation windows. Although these flaws may reduce the fatigue life they have been ignored since the importance of bone surface preparation on loosening is quantified in terms of the relative difference in fatigue life rather than the absolute number of cycles to failure. The windows serve as a venue to acquire images that encompass the interfaces and enable quantification of the relative displacement between the prosthesis, cement, and bone that result from axial loading of the prosthesis. Based on the specimen configuration there are four independent interface pairs that can be evaluated. The windows provide a direct view of the interfaces and represent a 2-D surface that supports application of DIC. Surface preparation is then required to minimize the glare of the titanium surface and to establish a high-contrast speckle field. For convenience of application, a white correction fluid was used to coat the surface, followed by a peripheral spray of black enamel paint to deposit the desired black dots.

After implanting the prosthesis and surface preparation the specimens were subjected to a monotonic axial load in seven equal increments ranging from $+100$ to -667 N. Loads were applied through the titanium prosthesis in a dedicated load frame while the specimen was supported vertically beneath the femoral wall. Note that a concentric axial load applied to the model joint while eccentric loading is more likely *in vivo*. The load configuration was simplified to enable a clear distinction of the effects from surface preparation on the loosening process. When the significance of bone surface prepara-

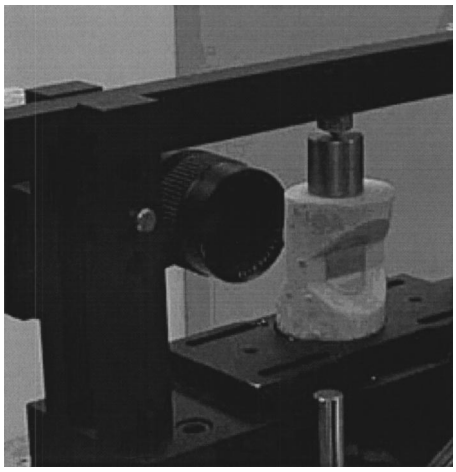

Fig. 8 Experimental setup for the evaluation of loosening in THR.

tion on loosening using axial loading is accomplished, future efforts will evaluate loosening under a more complete load distribution.

In all experiments, the digital camera was placed normal to the specimen surface at a distance capturing the bone/bone cement and bone cement/titanium prosthesis interfaces, as shown in Fig. 8. A digital image was captured at each increment of loading, compared with an image captured at no load, and then processed to determine the displacement distribution. The images comprised an area of 19×14 mm and were digitized into 2048×1536 pixels with 256 gray scales; the corresponding resolution in displacement was 10 μm/pixel. A typical full-field displacement distribution across the interface of a model joint replacement is shown in Fig. 9(a). The interfaces are clearly evident from the gray-scale map. The displacement distribution along a specific horizontal line extending across the two interfaces is shown in Fig. 9(b). The process was followed by fatigue loading of the model cemented joints with an axial load of $+100$ N to -667 N in increments of 1 million cycles. At the completion of 1 million cycles, the specimen was placed on the dedicated load frame, loaded axially, and the full-field displacement distribution was characterized using DIC.

The incremental fatigue and evaluation process enabled quantitative distinction of the initiation and progression of loosening in the cemented joints. More importantly, the mechanisms of loosening and the dependence on bone surface preparation and texture can be established from the full-field characterization of displacement. Preliminary attempts at characterizing the mechanisms of loosening in the cemented joints were conducting[35] using ESPI. However, the limited range of displacement measurement and difficulties with the surface preparation required for ESPI in the moist conditions proved DIC to be a much more suitable optical method. Therefore, in this application, DIC provides extremely valuable information over a range of deformation that cannot be acquired using other optical techniques. With further investigation it may be possible to identify surgical bone surface preparations that maximize the longevity of cemented total joint replacements.

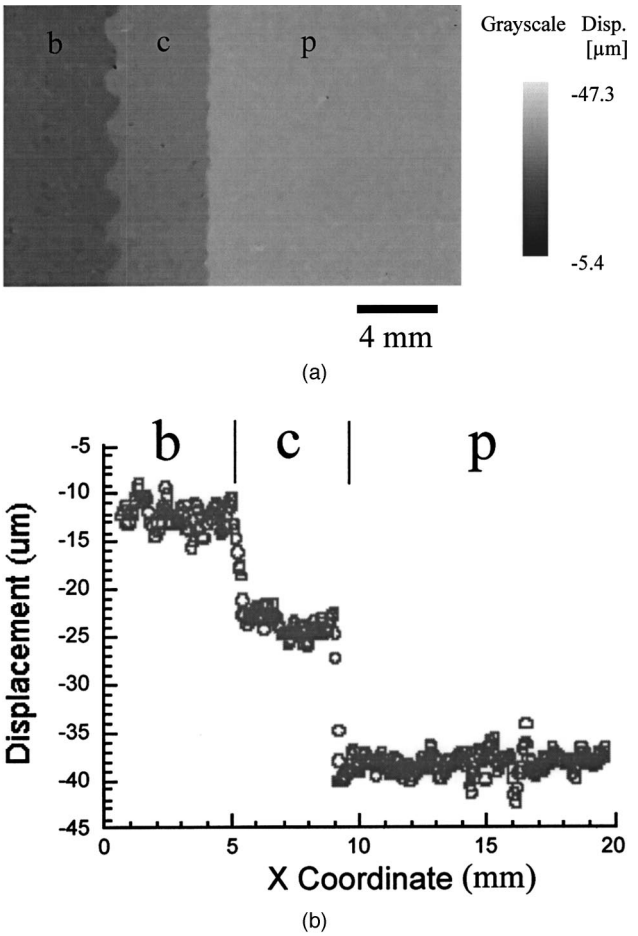

Fig. 9 Displacement distribution of a model implant system after fatigue loading (b=bone, c=cement, p=titanium prosthesis): (a) gray-scale map representing the axial displacement (parallel to the prosthesis) and (b) axial displacement distribution across the interfaces.

5 Summary

DIC is a robust optical method for displacement/strain measurement. It is comprised of a simple optical arrangement and is based on the principles of image recognition to compare images taken from the surface of a substrate. With proper surface preparation of the substrate, it can be applied to both engineering and biological materials. An approach for surface preparation was introduced that supports application of DIC to study the mechanical behavior of soft and hard hydrated tissues. Three examples were presented to highlight use of DIC in determining the mechanical properties of biological tissues. The examples involved materials with elastic modulus ranging from 200 kPa (arterial tissues) to 3 GPa (bovine hoof horn) and were evaluated under uniaxial tension up to 40% elongation. Spatial variations in the mechanical properties were evident from the full-field characterization of both tissues. An additional example was presented describing the use of DIC to quantify loosening in cemented THRs. Based on the breadth of applications, the value of DIC for biomedical research becomes apparent. The primary advantages of DIC over other alternatives is that the in-plane displacement (in two orthogonal directions) can be determined through the comparison of only two digital images and that it is a full-

field technique. The viscoelastic or viscoplastc properties of tissues can be examined using DIC with the appropriate timing between sequential frames. Though limited to *in vitro* evaluations thus far, DIC can serve as the benchmark for the other optical or nonoptical methods that are applied *in vivo*. If the natural texture of the substrate offers adequate contrast, which removes the need for surface preparation, DIC may find future applications for characterizing structural behavior *in vivo*. Microscopic DIC may also hold additional value in establishing structure/property relationships for soft and hard tissues.

Acknowledgments

This work was partially supported through a biomedical engineering research grant from the Maryland Chapter of the Arthritis Foundation and an equipment grant from the National Science Foundation (No. BES-9900196). The authors would also like to thank Mr. Dongliang Yang for help in conducting some of the experiments.

References

1. J. Woisetschlager, D. B. Shedffer, C. W. Loughry, K. Somasundaram, S. K. Chawla, and P. J. Wesolowski, ''Phase-shifting holographic interferometry for breast cancer detection,'' *Appl. Opt.* **33**(22), 5011–5015 (1994).
2. B. Ovryn, ''Holographic interferometry,'' *Crit. Rev. Biomed. Eng.* **16**(4), 269–322 (1989).
3. B. Ovryn, M. T. Manley, and L. S. Stern, ''Holographic interferometry: a critique of the technique and its potential for biomedical measurements,'' *Ann. Biomed. Eng.* **15**(1), 67–78 (1987).
4. S. Braun, J. A. Bottrel, K. G. Lee, J. J. Lunazzi, and H. L. Legan, ''The biomechanics of rapid maxillary sutural expansion,'' *Am. J. Orthod. Dentofacial Orthop.* **118**(3), 257–261 (2000).
5. A. Zentner, H. G. Sergl, and G. Filippidis, ''A holographic study of variations in bone deformations resulting from different headgear forces in a macerated human skull,'' *Angle Orthod.* **66**(6), 463–472 (1996).
6. M. K. Smolek, ''Holographic interferometry of intact and radially incised human eye-bank corneas,'' *J. Cataract Refractive Surg.* **20**(3), 277–286 (1994).
7. J. A. Brougher and J. D. Wood, ''Effects on drying and freezing on bovine bone,'' in *Proc. SEM Annu. Conf. on Theoretical, Experimental and Computational Mechanics*, p. 238, Milwaukee, WI (2002).
8. D. Zhang and D. Arola, ''Evaluating the elastic modulus of bone using electronic speckle pattern interferometry,'' *Exp. Tech.* **25**(5), 32–34 (2002).
9. R. Z. Wang and S. Weiner, ''Strain-structure relations in human teeth using Moire fringes,'' *J. Biomech.* **31**(2), 135–141 (1998).
10. D. Arola, J. Rouland, and D. Zhang, ''Fatigue and fracture of bovine dentin,'' *Exp. Mech.* **42**(4), 380–388 (2002).
11. A. Kishen and A. Asundi, ''Investigations of thermal property gradients in the human dentine,'' *J. Biomed. Mater. Res.* **55**(1), 121–130 (2001).
12. X. Niu, P. G. Ifju, J. R. Bianchi, and B. Wallace, ''A diffraction grating for compliant and porous materials,'' *Exp. Tech.* **24**(1), 27–30 (2000).
13. W. H. Peters and W. F. Ranson, ''Digital image technique in experimental stress analysis,'' *Opt. Eng.* **21**(3), 427–431 (1982).
14. T. C. Chu, W. F. Ranson, M. A. Sutton, and W. H. Peters, ''Applications of digital-image-correlation techniques to experimental mechanics,'' *Exp. Mech.* **25**(3), 232–244 (1985).
15. M. A. Sutton, Y. J. Chao, and J. S. Lyons, ''Computer vision methods for surface deformation measurements in fracture mechanics, novel experimental techniques in fracture mechanics,'' *ASME-AMD* **176**, 20317 (1993).
16. H. Lu, G. Vendroux, and W. G. Knauss, ''Surface deformation measurements of a cylindrical specimen by digital image correlation,'' *Exp. Mech.* **37**(4), 433–439 (1997).
17. W. Zhao and G. Jin, ''An experimental study on measurement of Poisson's ratio with digital correlation method,'' *J. Appl. Polym. Sci.* **60**(8), 1083–1088 (1996).
18. D. Zhang, X. Zhang, and G. Cheng, ''Compression strain measurement by digital speckle correlation,'' *Exp. Mech.* **39**(1), 62–65 (1999).
19. A. F. Bastawros, H. Bart-Smith, and A. G. Evans, ''Experimental analysis of deformation mechanisms in closed cell aluminum alloy foam,'' *J. Mech. Phys. Solids* **48**(2), 301–322 (2000).
20. D. M. McGowan, D. R. Ambur, T. G. Hanna, and S. R. McNeill, ''Evaluating the compressive response of notched composite panels using full-field displacements,'' *J. Aircr.* **38**(1), 122–129 (2001).
21. W. Tong, ''Detection of plastic deformation patterns in a binary aluminum alloy,'' *Exp. Mech.* **37**(4), 452–459 (1997).
22. B. Wattrisse, A. Chrysochoos, J.-M. Muracciole, and M. Nemoz-Gaillard, ''Analysis of strain localization during tensile tests by digital image correlation,'' *Exp. Mech.* **41**(1), 29–39 (2001).
23. H. A. Bruck, S. R. McNeill, M. A. Sutton, and W. H. Peter, ''Digital image correlation using Newton-Raphson method of partial differential correlation,'' *Exp. Mech.* **29**(3), 261–267 (1989).
24. D. Zhang and D. Arola, ''A new fast-search strategy for digital image correlation,'' in *Proc. SEM Annu. Conf. on Theoretical, Experimental and Computational Mechanics*, Paper 80, Milwaukee, WI (2002).
25. D. Zhang, C. D. Eggleton, and D. Arola, ''Evaluating the mechanical behavior of the arterial tissue using digital image correlation,'' *Exp. Mech.* **42**(4), 409–416 (2002).
26. D. Zhang, D. Arola, and C. D. Eggleton, ''Measurement of Poisson's ratio of bovine aorta using digital image correlation,'' in *Proc. 2nd BMES/IEEE Joint Meeting*, pp. 1276–1277 Houston, TX (2002).
27. D. Zhang, C. Eggleton, and D. Arola, ''An application of digital image correlation to bovine aorta,'' in *Proc. SEM Annu. Conf. on Theoretical, Experimental and Computational Mechanics*, Paper 194, Milwaukee, WI (2002).
28. D. Zhang, S. Davis, C. Eggleton, and D. Arola, ''Examining the constitutive behavior of bovine aorta using digital image correlation,'' in *Proc. Annu. Meeting of the Society of Biomaterials*, p. 315, Tampa, FL (2002).
29. J. Zhou and Y. C. Fung, ''The degree of nonlinearity and anisotropy of blood vessel elasticity,'' *Proc. Natl. Acad. Sci. U.S.A.* **94**(26), 14255–14260 (1997).
30. J. D. Humphrey, D. L. Vawter, and R. P. Vito, ''Quantification of strains in biaxially tested soft tissues,'' *J. Biomech.* **20**(1), 59–65 (1987).
31. F. H. Silver, D. L. Christiansen, and C. M. Buntin, ''Mechanical properties of the aorta: a review,'' *Crit. Rev. Biomed. Eng.* **17**(4), 323–358 (1989).
32. Y. C. Fung, *Biomechanics, Mechanical Properties of Living Tissues*, 2nd ed., pp. 321–369, Springer, New York (1993).
33. D. Arola, D. Zhang, R. Reprogel, W. Zheng, P. Rajkondawar, and U. Tasch, ''The influence of moisture on the elastic properties of bovine hoof horn,'' in *Proc. 21st Southern Biomedical Engineering Conf.*, pp. 147–149, Bethesda, MD, (2002).
34. P. Rajkondawar, D. Zhang, D. Arola, and U. Tasch, ''Mechanical characterization of bovine hooves: comparing healthy and ailing hooves,'' in *Proc. SEM Annu. Conf. on Theoretical, Experimental and Computational Mechanics*, p. 256 Milwaukee, WI (2002).
35. D. T. Yang, K. A. Stoffel, D. Zhang, and D. Arola, ''Loosening in total hip arthroplasty: an evaluation using DIC and ESP,'' in *Proc. SEM Annu. Conf. on Theoretical, Experimental and Computational Mechanics*, p. 75, Milwaukee, WI (2002).
36. D. T. Yang, D. Zhang, K. A. Stoffel, and D. Arola, ''The mechanics of loosening in cemented total hip replacements resulting from fatigue loads,'' in *Proc. Annu. Meeting of the Society of Biomaterials*, p. 546, Tampa, FL (2002).